Thermal Decomposition of Tin Tetrachloride Based on Cl- and Sn-Concentration Measurements

Kazuo Takahashi, Andreas Kunz, Dirk Woiki, and Paul Roth*

Institut für Verbrennung und Gasdynamik, Gerhard-Mercator-Universität Duisburg, 47048 Duisburg, Germany

Received: November 10, 1999; In Final Form: March 7, 2000

The kinetics of the thermal decomposition of tin tetrachloride has been studied experimentally and theoretically. Ab initio MO calculations showed that $SnCl_4$ finally decomposed into $Sn(^3P)$ and four chlorine atoms through four subsequent Sn−Cl bond dissociation channels. Two sets of kinetic experiments were performed using a shock tube equipped with atomic resonance absorption spectroscopy (ARAS). Chlorine atoms were first measured over the temperature range of 1250−1700 K and the total density range of 1.7×10^{18} to 8.9×10^{18} molecules cm^{-3}. The rate coefficient for the initial reaction step, $SnCl_4$ (+M) → $SnCl_3(^2A_1)$ + Cl (+M) (eq 1a), was found to be in the falloff region fairly close to the low-pressure limit under the present conditions. The second-order rate coefficient based on the Cl-atom measurements was determined to be $k_{1a}^{2nd} = 10^{-5.37\pm0.62}$ exp[−(285 ± 18) kJ mol^{-1}/RT] cm^3 $molecule^{-1}$ s^{-1} (error limits at the 2 standard deviation level). The second group of experiments was carried out by detecting tin atoms over the temperature range of 2250−2950 K and at a total density of 3.2×10^{18} molecules cm^{-3}. The second-order rate coefficients for the subsequent reaction steps: $SnCl_2(^1A_1)$ (+M) → $SnCl(^2\Pi)$ + Cl (+M) (eq 3a) and $SnCl(^2\Pi)$ (+M) → $Sn(^3P)$ + Cl (+M) (eq 4a) were obtained to be $k_{3a}^{2nd} = 10^{-8.36\pm0.86}$ exp[−(310 ± 42) kJ mol^{-1}/RT] cm^3 $molecule^{-1}$ s^{-1} and $k_{4a}^{2nd} = 10^{-9.50\pm0.78}$ exp[−(265 ± 40) kJ mol^{-1}/RT] cm^3 $molecule^{-1}$ s^{-1}, respectively. The Rice−Ramsperger−Kassel−Marcus (RRKM) calculations including variational transition state theory were also applied for reactions 1a and 3a. Structural parameters and vibrational frequencies of the reactants and transition states required for the RRKM calculations were obtained from the ab initio MO calculations. Energy barriers of the reactions, E_0's, which are the most sensitive parameters in the calculations, were adjusted until the RRKM rate coefficients matched the observed ones. These fittings yielded $E_{0,1a} = 326$ kJ mol^{-1} for reaction 1a and $E_{0,3a} = 368$ kJ mol^{-1} for reaction 3a, in good agreement with the Sn−Cl bond dissociation energies of $SnCl_4$ and $SnCl_2$, demonstrating that the experimental data for k_{1a} and k_{3a} were theoretically reasonable and acceptable.

Introduction

Tin dioxide (SnO_2) is an industrially important material with the characteristics of high electric conductivity and high transmissivity.[1−3] Its applications range from use as a transparent electrode in photovoltaic cells, and imaging and display devices, to use as an energy-conserving coating on windows and light bulbs. Tin dioxide is also used as a gas sensor, because its surface resistance is sensitive to gas adsorption. The process used for SnO_2 synthesis depends on the technical application. When thin films with uniform thickness or fine particles with uniform size are needed, SnO_2 is often produced in high-temperature gas-phase processes, e.g., chemical vapor deposition (CVD), high-temperature flow reactors, and flames. However, the optimum reaction conditions to control these gas-phase processes still have to be found empirically. To solve this problem, the knowledge about reaction mechanism and rate coefficients during the SnO_2 synthesis are necessary.

Normally, chlorides and organic compounds such as tin tetrachloride, tetramethyltin, and dimethyldichlorotin are used as Sn precursors for the gas-phase synthesis. A few kinetic studies on the reactions of Sn precursors were previously reported, although numerous reactions of electronically ground-state tin atoms, which are an intermediate species during the SnO_2 synthesis, e.g., $Sn(^3P) + O_2$,[4−7] $Sn(^3P) + N_2O$,[4−6,8] $Sn(^3P) + CO_2$,[4,7] $Sn(^3P)$ + hydrocarbons,[4] were investigated. As for the Sn precursor reactions, the thermal decompositions of $Sn(CH_3)_4$ and $(CH_3)_2SnCl_2$ were first studied by Price et al.[9,10] in a toluene carrier flow system. The rate coefficients for the reactions $Sn(CH_3)_4 \rightarrow Sn(CH_3)_3 + CH_3$ and $(CH_3)_2SnCl_2 \rightarrow CH_3SnCl_2 + CH_3$ were determined to be $k^{1st} = 10^{15.7}$ exp[−270 kJ mol^{-1}/RT] and $10^{13.5}$ exp[−235 kJ mol^{-1}/RT] s^{-1} over the temperature ranges of 803−941 K and 827−961 K, respectively. In other works,[11−13] the kinetics of the $Sn(CH_3)_4$ thermal decomposition was reported. However, no kinetic data for the thermal decomposition of tin tetrachloride, which is the most important Sn precursor, are published.

In our laboratory, the gas-phase reactions of some metal chlorides used as Si and Ti precursors were previously studied.[14−16] This series of work is now continued by the thermal decomposition of $SnCl_4$, which is regarded as a first step to clarify the reaction mechanism of the SnO_2 synthesis from $SnCl_4$. Possible channels for the thermal decomposition of $SnCl_4$ were theoretically examined by ab initio MO calculations. Furthermore, two sets of kinetic experiments were performed using a shock tube equipped with atomic resonance absorption spectroscopy (ARAS). Chlorine atoms were first measured in relatively low-temperature experiments to study the kinetics of the initial reaction step:

* Corresponding author. Phone: +49-203-379 3417. Fax: +49-203-379 3087. E-mail: roth@ivg.uni-duisburg.de.

10.1021/jp993985j CCC: $19.00 © 2000 American Chemical Society
Published on Web 05/13/2000

$$SnCl_4\ (+M) \rightarrow SnCl_3(^2A_1) + Cl\ (+M) \qquad (1a)$$

The second group of experiments was carried out at higher temperatures by detecting tin atoms to follow the subsequent reaction steps:

$$SnCl_2(^1A_1)\ (+M) \rightarrow SnCl(^2\Pi) + Cl\ (+M) \qquad (3a)$$

$$SnCl(^2\Pi)\ (+M) \rightarrow Sn(^3P) + Cl\ (+M) \qquad (4a)$$

The Rice−Ramsperger−Kassel−Marcus (RRKM) calculations including variational transition state theory were also applied to confirm these experimental results.

Experimental Section

Shock Tube. All experiments were performed behind reflected shock waves in a stainless steel shock tube with an internal diameter of 79 mm. This shock tube consists of a 3.5 m long driver section and a 5.7 m long test section which are separated by an aluminum diaphragm. The test section was evacuated by a turbomolecular pump to pressures down to 5×10^{-7} mbar. Residual gases in the shock tube were analyzed by a quadrupole mass spectrometer and were found to be practically free of hydrocarbons. To measure the incident shock velocity, three gold-resistance-type transducers were placed in the shock tube wall at 15 cm intervals near the end of the test section. Temperature and pressure of shock-heated test gas were calculated from the measured incident shock velocity using standard methods. Further details of the shock-tube apparatus are given elsewhere.[17,18]

Optical System and Calibration. Time-resolved concentrations of electronically ground-state Cl ($3p^5\ ^2P^0_{3/2}$) and Sn ($5p^2\ ^3P_0$) atoms were monitored by atomic resonance absorption spectroscopy (ARAS). As a light source of Cl atom ARAS, a microwave discharge lamp (35 W) was used, in which a mixture of 0.1% Cl_2/He was flowing at a pressure of 5 mbar. The resonant radiation from the lamp passed through two LiF windows (1 mm thickness) mounted on the shock tube walls at a position of 1.4 cm apart from the end plate. The transmitted light was isolated by a 1 m vacuum-UV monochromator (McPherson GCA-225), which was evacuated to a pressure less than 2×10^{-7} mbar, and detected by a solar-blind photomultiplier (EMR 542G-08-18). Perpendicular to the Cl atom detection system, a Sn hollow cathode lamp (Hamamatsu Photonics L233-50NQ) operated by a pulsed power source, a 25 cm monochromator (Jarrell Ash), and a UV−vis photomultiplier (Hamamatsu Photonics 1P28) were arranged to measure Sn atom absorption. This crossing optical setup enables us to monitor Cl and Sn atoms simultaneously. The wavelengths of the Cl and Sn resonance lines used in the present study were 134.7 nm ($4s^2P_{3/2} \leftarrow 3p^5\ ^2P^0_{3/2}$) and 286.3 nm ($6s^3P^0_1 \leftarrow 5p^2\ ^3P_0$), because their sensitivities were the highest of all Cl and Sn resonance lines.

Calibration experiments were performed behind reflected shock waves by using 0.5−4 ppm of CH_3Cl/Ar mixtures at 2500−3000 K and 0.05−5 ppm $Sn(CH_3)_4$/Ar mixtures at 2800−3800 K for Cl- and Sn atom ARAS, respectively. Methyl chloride completely decomposes into CH_3 and Cl within 700 μs at 1800 K.[19] On the other hand, tetramethyltin finally decomposes into $Sn(^3P)$ and four methyl radicals at high temperatures through the rate-determining initial step $Sn(CH_3)_4 \rightarrow Sn(CH_3)_3 + CH_3$ and three subsequent fast Sn−C bond dissociation channels. From the kinetic data,[20] 99.8% of $Sn(CH_3)_4$ is calculated to decompose into $Sn(^3P)$ and the other fragments within 10 ns at 2800 K. Therefore, calibration curves for both diagnostics can be obtained by relating measured steady-state absorptions to known initial concentrations of CH_3-Cl and $Sn(CH_3)_4$. The calibration results are summarized in the upper part of Figure 1 for Cl atoms and in the lower part for Sn atoms. The sensitivities are almost equal between the Cl and Sn atom detection systems. In both cases, the Lambert−Beer law cannot be applied, due to self-absorption or self-reversal. Assuming the modified Lambert−Beer equation

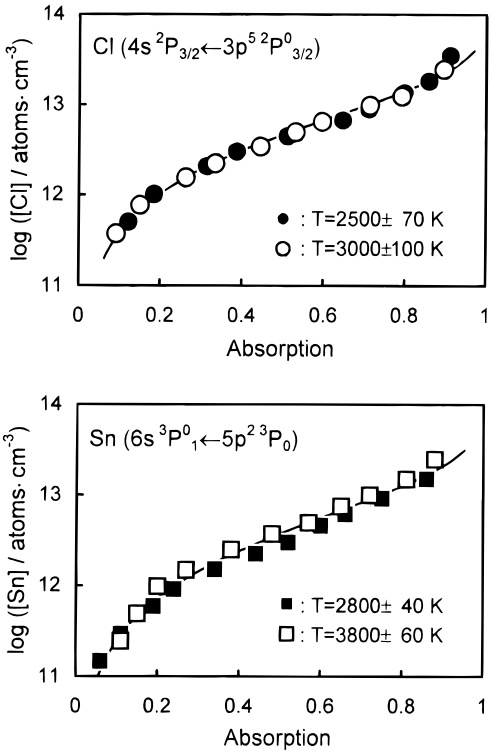

Figure 1. Calibration curves for Cl atoms at 134.7 nm (upper part) and Sn atoms 286.3 nm (lower part). The solid lines are least-squares fits to the data (see text).

$$1 - \frac{I}{I_0} = 1 - \exp\{-\sigma_0 l[X]^\gamma\}$$

(l is optical path length (=7.9 cm)) the two parameters σ_0 and γ were determined for both atoms by least-squares methods as follows:

$$\sigma_0(Cl) = 10^{-10.60\pm0.40}\ cm^{1.25}\ atom^{-0.75},$$
$$\gamma(Cl) = 0.753 \pm 0.031 \text{ at } 134.7 \text{ nm}$$

$$\sigma_0(Sn) = 10^{-9.78\pm0.47}\ cm^{1.08}\ atom^{-0.69},$$
$$\gamma(Sn) = 0.694 \pm 0.038 \text{ at } 286.3 \text{ nm}$$

The fitting curves calculated from these expressions approximate the experimental data very well; see solid lines in Figure 1.

Measurements and Gases. Two sets of kinetic experiments were performed in the present study. Chlorine atoms were first measured at relatively low temperatures to study the kinetics of the initial reaction step of the $SnCl_4$ thermal decomposition. The second group of experiments was carried out at higher temperatures by detecting tin atoms to follow the subsequent reaction steps. Details of the experimental conditions used are summarized in Table 1.

Test gas mixtures of $SnCl_4$ highly diluted in argon were prepared manometrically in a stainless steel storage cylinder.

TABLE 1: Experimental Conditions

experiment	mole fraction of $SnCl_4$ diluted in Ar/ppm	temp/K	total density/10^{18} molecules cm^{-3}	reaction
Cl atom measurements	0.2−9	1250−1700	1.7 ± 0.2, 8.9 ± 0.9	initial step in $SnCl_4$ thermal decomposition
Sn atom measurements	0.7−4	2250−2950	3.2 ± 0.5	subsequent decomposition steps

TABLE 2: Enthalpies of Possible Reaction Channels during $SnCl_4$ Thermal Decomposition Calculated at MP2/3-21G(d) Level

reaction channel		$\Delta H°$(0 K)/kJ mol^{-1}
$SnCl_4$(+M)	→ $SnCl_3(^2A_1)$ + Cl (+M) (1a)	362
	→ $SnCl_2(^1A_1)$ + Cl_2 (+M) (1b)	397
$SnCl_3(^2A_1)$(+M)	→ $SnCl_2(^1A_1)$ + Cl (+M) (2a)	206
	→ $SnCl_2(^3B_1)$ + Cl (+M) (2b)	432
	→ $SnCl(^2\Pi)$ + Cl_2 (+M) (2c)	415
$SnCl_2(^2A_1)$(+M)	→ $SnCl(^2\Pi)$ + Cl (+M) (3a)	380
	→ $Sn(^1D)$ + Cl_2 (+M) (3b)	680
$SnCl(^2\Pi)$(+M)	→ $Sn(^3P)$ + Cl (+M) (4a)	344
	→ $Sn(^1D)$ + Cl (+M) (4b)	470

Purities of the samples used were >99.999% for argon and >99% for $SnCl_4$. Tin tetrachloride, which is liquid at standard conditions, was carefully injected and evaporated in a separate stainless steel vessel.

There was an experimental difficulty that a small amount of $SnCl_4$ disappeared in the stainless steel storage cylinder due to adsorption of $SnCl_4$ at the walls. Because of this phenomenon, the initial concentration of $SnCl_4$ could not be determined precisely from the partial pressure of $SnCl_4$ introduced. So, just before every kinetic experiment, a Cl atom measurement was carried out at high temperatures above 4000 K, in order to check the gas-phase mole fraction of $SnCl_4$. Chlorine atoms rapidly increased to reach a constant value immediately after the arrival of a reflected shock wave. At T > 4000 K, $SnCl_4$ completely decomposes into $Sn(^3P)$ and four chlorine atoms regardless of reaction pathway or rate. The mole fraction of $SnCl_4$ in the mixture, $X(SnCl_4)$, can be determined by the following formula:

$$X(SnCl_4) = \frac{1}{4}\frac{[Cl]_{ss}}{[M]}$$

where $[Cl]_{ss}$ and [M] are the Cl atom concentration at steady state obtained from the ARAS signal and the total concentration behind the reflected shock wave, respectively. The adsorption of $SnCl_4$ on stainless steel surfaces is not very fast. Therefore, the adsorption on the inner walls of the shock tube during test gas introduction and shock generation is negligible.

Results and Discussion

Theoretical Examination of Reaction Channels. To examine possible channels for the thermal decomposition of $SnCl_4$, thermochemical data for the reactants and products are necessary, which are mostly not available. So, ab initio MO calculations were performed using the Gaussian 94 program.[21] Enthalpies of the possible reaction channels calculated at MP2/3-21G(d) level are summarized in Table 2. The comparison with some experimental data[22,23] confirms that the MP2/3-21G(d) calculations systematically overestimate these reaction enthalpies by 5 to 15%, because of utilizing small basis sets. As found from Table 2, the reaction enthalpy of Cl formation by reaction 1a is 35 kJ mol^{-1} lower than that of Cl_2 elimination by reaction 1b. This difference results in a ratio of $k_{1b}/k_{1a} = 0.04-0.08$ in the present experimental temperature range, assuming that the energy barriers of reactions 1a and 1b are equal to their reaction enthalpies and that both preexponential factors are identical.

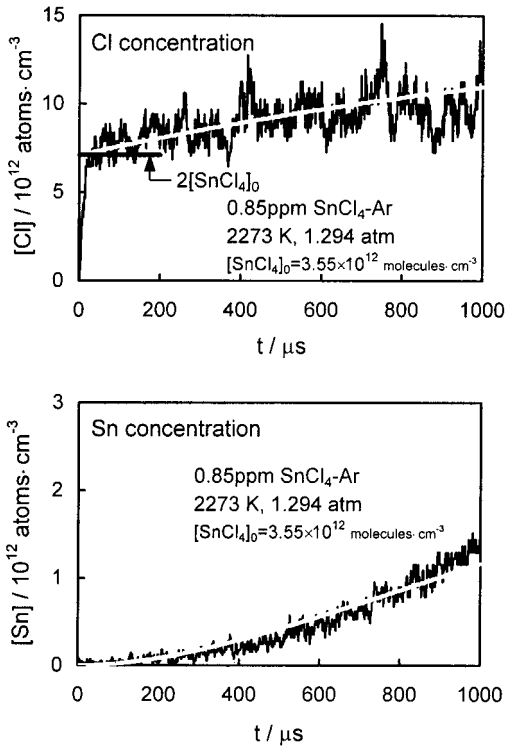

Figure 2. Typical measured concentration profiles of Cl (upper part) and Sn atoms (lower part) in a $SnCl_4$−Ar mixture heated to a temperature of 2273 K. The white lines denote profiles calculated by using the simplified reaction model consisting of reactions 1a, 2a, 3a, and 4a.

Additionally, reaction 1b has energy barriers not only for the forward but also for the reverse directions,[24] because reaction 1b proceeds via a three-centered transition state configuration, resulting in a forward barrier of reaction 1b being higher than the reaction enthalpy. From this consideration, it can be concluded that reaction 1b is negligible as the initial step of the $SnCl_4$ pyrolysis even if the accuracies of the calculated reaction enthalpies are not so high. Furthermore, the calculations show that the other Sn−Cl bond dissociation channels (2a), (3a), and (4a) are the energetically most favorable ones in the subsequent decomposition pathways so that $SnCl_4$ finally decomposes into $Sn(^3P)$ and four chlorine atoms.

Kinetics of the Initial Decomposition Step. Figure 2 shows concentration profiles of Cl and Sn atoms in a $SnCl_4$−Ar mixture at the temperature corresponding to the lower limit of Sn atom formation. At this temperature, the formation of chlorine atoms can be divided into two stages: fast Cl atom formation within 30 μs followed by a relatively slow further increase. Such behavior can be understood as the rapid formation of $SnCl_2(^1A_1)$ and two chlorine atoms through reactions 1a and 2a, because the measured Cl atom concentration reaches twice the initial concentration of $SnCl_4$, and Sn atoms are not detected. During the subsequent time, reactions 3a and 4a are initiated to produce both Cl and Sn atoms slowly. This suggestion is confirmed by the ab initio calculation. As shown in Table 2, the barrier of reaction 2a is relatively low so that reaction 2a immediately follows reaction 1a, leading to the formation of

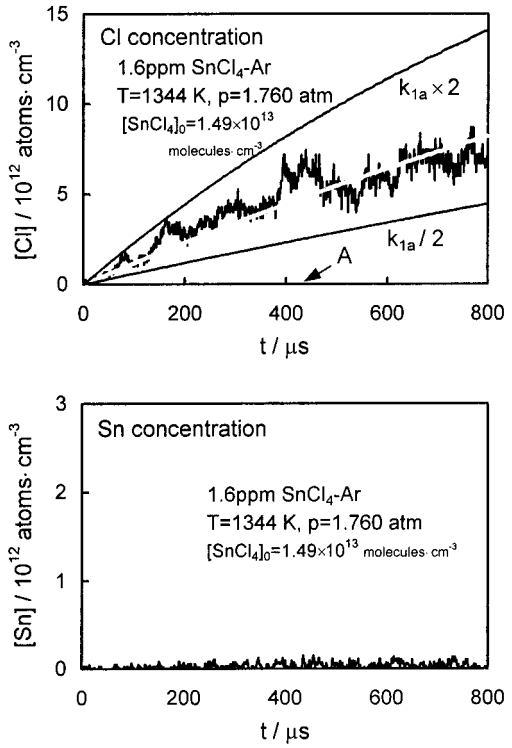

Figure 3. Typical measured concentration profiles of Cl (upper part) and Sn atoms (lower part) in a $SnCl_4-Ar$ mixture heated to a temperature of 1344 K. The white and the two black lines in the upper part denote profiles calculated by varying the rate coefficient for reaction 1a. Line A being identical with the horizontal axis is the Cl atom concentration calculated with reactions 1b and S1 (see text).

$SnCl_2(^1A_1) + 2Cl$ from $SnCl_4$. On the other hand, the barrier of the subsequent reaction 3a is relatively high so that Cl atoms are slowly formed through reactions 3a and 4a at this temperature.

On the basis of this discussion, shock-tube experiments were performed at lower temperatures of 1250−1700 K, in order to study the kinetics of the initial part of the $SnCl_4$ thermal decomposition. Figure 3 shows typical concentration profiles of Cl and Sn atoms. Chlorine atoms increase monotonically, but no tin atoms are detected during the reaction time of about 800 μs. These results show that reactions 3a and 4a have no influence on Cl-atom formation in this temperature range. As reaction 2a is considered to be much faster than reaction 1a by the theory, the steady-state approximation can be applied to the $SnCl_3$ concentration. Under the present conditions, the Cl atom concentration at time t, $[Cl]_t$, can be expressed as follows:

$$[Cl]_t = 2[SnCl_4]_0\{1 - \exp(-k_{1a}^{1st}t)\}$$

The first-order rate coefficient for reaction 1a, k_{1a}^{1st}, was determined by fitting calculated Cl atom concentrations to observed ones; see three lines in the upper part of Figure 3. The Arrhenius plot of k_{1a}^{1st} obtained by this method is shown in Figure 4, which obviously depends on total concentration [M]. So, the second-order rate coefficient k_{1a}^{2nd} calculated by the relation $k_{1a}^{2nd} = k_{1a}^{1st}/[M]$ is plotted in Figure 5. For the two different total concentrations, the values of k_{1a}^{2nd} follow a single straight line. This result shows that the rate coefficient for reaction 1a is fairly close to the low-pressure limit under the present experimental conditions. However, the experiments were performed in a relatively narrow range of total density, so that they did not have enough sensitivity to specify whether the reaction was in the true low-pressure limit or not. A least-

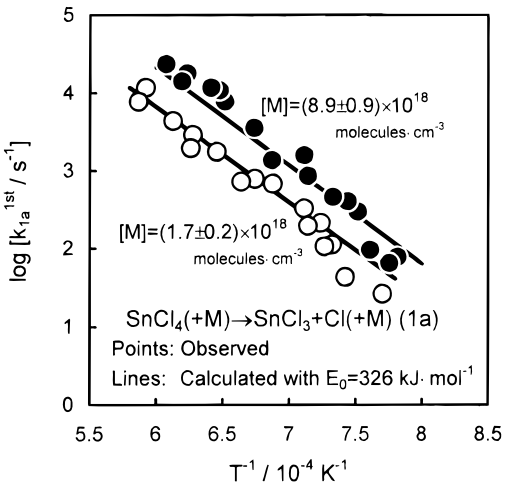

Figure 4. Arrhenius plot of the first-order rate coefficient for reaction 1a. (○) and (●) denote the results measured at [M] = (1.7 ± 0.2) × 10^{18} molecules cm^{-3} and [M] = (8.9 ± 0.9) × 10^{18} molecules cm^{-3}, respectively. The solid lines show the RRKM results calculated with $E_{0,1a}$ = 326 kJ mol^{-1} (see text).

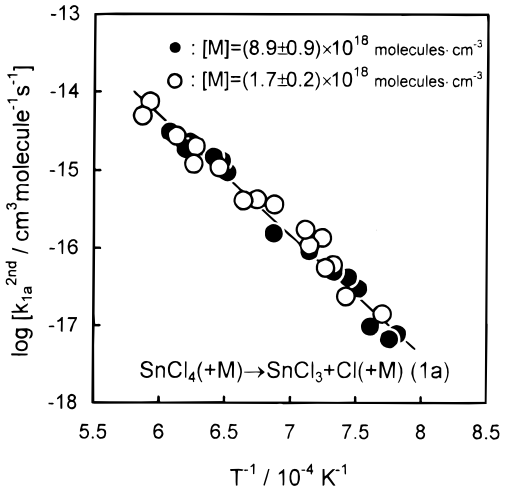

Figure 5. Arrhenius plot of the second-order rate coefficient for reaction 1a. (○) and (●) denote the results measured at [M] = (1.7 ± 0.2) × 10^{18} molecules cm^{-3} and [M] = (8.9 ± 0.9) × 10^{18} molecules cm^{-3}, respectively.

squares fit yielded the following Arrhenius expression over the temperature range of 1250−1700 K:

$$k_{1a}^{2nd} = 10^{-5.37\pm0.62} \times \exp[-(285 \pm 18)\ \text{kJ mol}^{-1}/RT]\ \text{cm}^3\ \text{molecule}^{-1}\ \text{s}^{-1}$$

where the error limits are at the two standard deviation level. If this expression is assumed to be the low-pressure limit rate coefficient, the preexponential factor seems to be too large. Therefore, we can conclude that reaction 1a is in the falloff region but fairly close to the low-pressure limit.

The mixtures of $SnCl_4$ used were highly diluted in argon to avoid secondary reactions. Although it is most unlikely that side reactions are of importance under these conditions, the contributions of some reactions should be discussed here. The side reactions which may affect the determination of k_{1a} are $SnCl_4 + Cl \rightarrow SnCl_3 + Cl_2$ (S1) and $SnCl_3 + SnCl_3 \rightarrow$ products (S2). Reaction S1 is endothermic and its enthalpy at 0 K is examined to be 122 kJ mol^{-1} from the ab initio MO calculations. The collision theory gives $k_{S1} = 5.3 \times 10^{-15}$ and 9.9×10^{-14} cm^3 $molecule^{-1}$ s^{-1} at 1250 and 1700 K, respectively. Since the

maximum concentration of Cl atoms formed during the reaction time, $[Cl]_{max}$, is about 1×10^{13} atoms cm^{-3}, the upper limits for the ratios of reaction rates of reactions S1 and 1a, $k_{S1}[Cl]_{max}/k_{1a}^{2nd}$ [M], can be estimated to be 3×10^{-3} and 8×10^{-5} at 1250 and 1700 K, respectively. This evaluation shows that reaction S1 is much slower than reaction 1a and therefore negligible. On the other hand, reaction S2 is exothermic. The upper limits for the ratios of reaction rates of reactions S2 and 1a, $k_{S2}[SnCl_3]_{max}/k_{1a}^{2nd}$ [M], can also be calculated from the Lennard-Jones collision frequency and the maximum concentration of $SnCl_3$ to be in the range of 1×10^{-2} to 2×10^{-5}. Therefore, both reactions S1 and S2 have no influence on the determination of k_{1a}.

From the ab initio calculations, reaction 1a was examined to be favored compared to the Cl_2-elimination channel (1b). This theoretical consideration can be confirmed by the measured Cl atom concentration profiles. If the main initial step of the $SnCl_4$ thermal decomposition is reaction 1b, instead of (1a), the detected chlorine atoms should be formed through the reaction $Cl_2 + M \rightarrow Cl + Cl + M$ (S3). As an extreme example, the rate of reaction 1b is assumed to be much faster than that of reaction S3. The concentration of Cl atoms formed through reactions 1b and S3, $[Cl]_t^{S3}$, can then be expressed as follows:

$$[Cl]_t^{S3} = 2[SnCl_4]_0\{1 - \exp(-k_{S3}[M]t)\}$$

where k_{S3} is the bimolecular rate coefficient for reaction S3. The data of k_{S3} were reported by numerous workers.[25−31] Baulch et al.[32] recommended the following Arrhenius expression in their review article:

$$k_{S3} = 10^{-10.41} \exp[-197 \text{ kJ mol}^{-1}/RT] \text{ cm}^3 \text{ molecule}^{-1} \text{ s}^{-1}$$

The time after which the Cl atoms reach 10% of the initial concentration of $SnCl_4$ can be calculated from this formula to be 6200 μs at 1344 K. The experimental result is only 130 μs; see the upper part of Figure 3. This means that the formation rate of Cl atoms through reactions 1b and S3 is too slow to explain the measured Cl atom concentration. Therefore, it is absolutely impossible that reaction 1b is the dominant channel.

The rate coefficient for reaction 1a cannot be compared with previous data, because it has first been measured in the present study. A similar kinetic study on the thermal decomposition of $SiCl_4$ has been performed in our laboratory. Silicon belongs to the same group (group 14) as tin, so that the mechanism for the thermal decomposition of $SiCl_4$ is very similar to that of $SnCl_4$. The second-order rate coefficient for the reaction:

$$SiCl_4 (+M) \rightarrow SiCl_3 + Cl (+M) \qquad \text{(Si-1a)}$$

was reported as follows:[16]

$$k_{Si-1a}^{2nd} = 10^{-6.94} \exp[-314 \text{ kJ mol}^{-1}/RT] \text{ cm}^3 \text{ molecule}^{-1} \text{ s}^{-1}$$

The apparent activation energy of k_{Si-1a}^{2nd} is higher than that of k_{1a}^{2nd}. This tendency can qualitatively be explained by the difference in dissociation energies between Si−Cl and Sn−Cl bonds.

Kinetics of the Subsequent Decomposition Steps. To study the kinetics of the subsequent decomposition reactions 3a and 4a, Sn atom measurements were performed at higher temperatures of 2250−2950 K. Figure 6 shows a typical concentration profile of Sn atoms, which increases gradually to reach finally the initial concentration of $SnCl_4$. This indicates that the thermal decomposition of $SnCl_4$ is completed within the reaction time of about 1000 μs. To determine the rate coefficients for reactions 3a and 4a, Sn atom concentration was calculated based on the simplified reaction scheme consisting of reactions 1a, 2a, 3a, and 4a and compared with observed one. As a measure of fitting quality, the sum of squared deviation between observed and calculated Sn atom concentrations, $F^2(k_{3a},k_{4a})$, was calculated as functions of both rate coefficients k_{3a} and k_{4a}:

$$F^2(k_{3a},k_{4a}) = \int_t \{[Sn](t)_{obs} - [Sn](t,k_{3a},k_{4a})_{calc}\}^2 \, dt$$

As the value of F^2 becomes smaller, the fitting can be judged to be better. A typical distribution diagram of F^2 is shown in Figure 7. When k_{3a} is fixed at a certain value, the minimum point for F^2, i.e., $F_{min}^2(k_{3a}=\text{fix})$, can always be found at an appropriate k_{4a}. Since the absolute values of $F_{min}^2(k_{3a}=\text{fix})$ depend on the combination of k_{3a} and k_{4a}, we can simultaneously determine these rate coefficients from only Sn atom profiles by determining the minimum point for $F_{min}^2(k_{3a}=\text{fix})$, as shown with an arrow in Figure 7.

Sensitivity analyses were performed with k_{1a}, k_{3a}, and k_{4a} determined in the present study. The CHEMKIN-II[33] and SENKIN[34] program codes were used in the calculation. An example is shown is Figure 8. The Sn atom concentration is

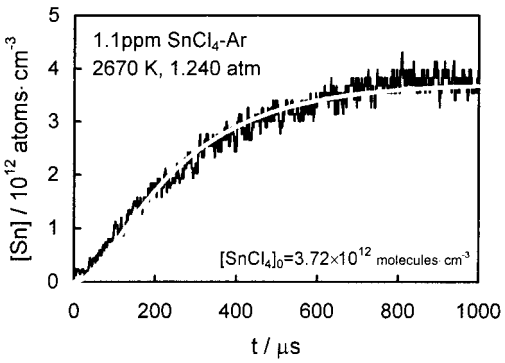

Figure 6. Typical measured concentration profile of Sn atoms in a $SnCl_4$−Ar mixture heated at a temperature of 2670 K. The white line denotes a profile calculated by using the simplified reaction model consisting of reactions 1a, 2a, 3a, and 4a.

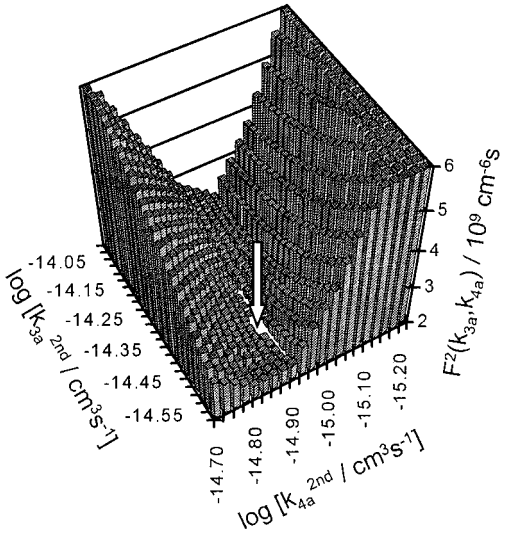

Figure 7. Sum of squared deviation between observed and calculated Sn atom concentrations as functions of both rate coefficients for reactions 3a and 4a. 1.1 ppm $SnCl_4$−Ar mixture; $T = 2670$ K; $P = 1.240$ atm.

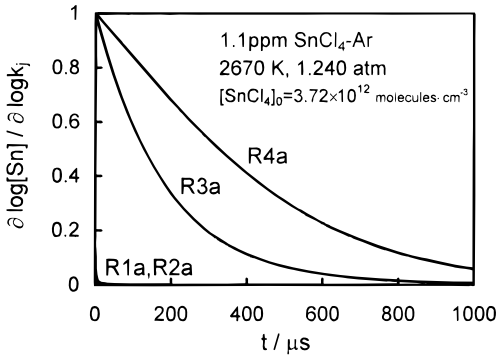

Figure 8. Sensitivity analysis of rate coefficients for Sn atom formation in a $SnCl_4-Ar$ mixture heated to a temperature of 2670 K.

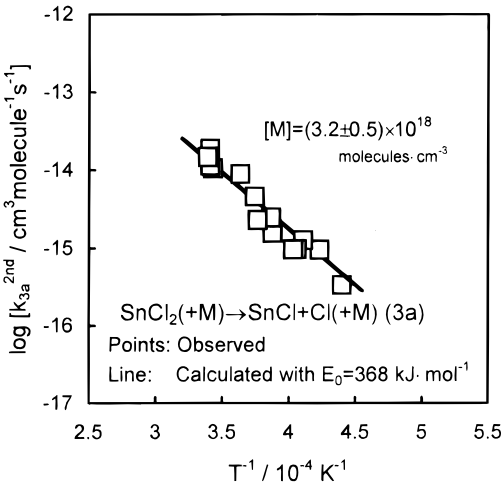

Figure 9. Arrhenius plot of the second-order rate coefficient for reaction 3a measured at [M] = (3.2 ± 0.5) × 10^{18} molecules cm^{-3}. The solid line shows the RRKM result calculated with $E_{0,3a}$ = 368 kJ mol^{-1} (see text).

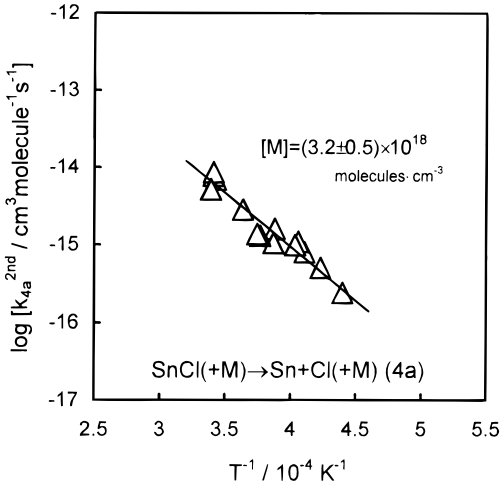

Figure 10. Arrhenius plot of the second-order rate coefficient for reaction 4a measured at [M] = (3.2 ± 0.5) × 10^{18} molecules cm^{-3}.

sensitive enough to determine the kinetic data of reactions 3a and 4a, while the initial decomposition reactions 1a and 2a have little sensitivity. Furthermore, the ratio of the sensitivities for rate coefficients k_{3a} and k_{4a} coefficients changes during reaction time. These are the reasons why k_{3a} and k_{4a} can simultaneously be determined by the above procedure. Figures 9 and 10 show Arrhenius plots of the second-order rate coefficients for reactions 3a and 4a, respectively. Least-squares fits resulted in the following Arrhenius expressions over the temperature range of

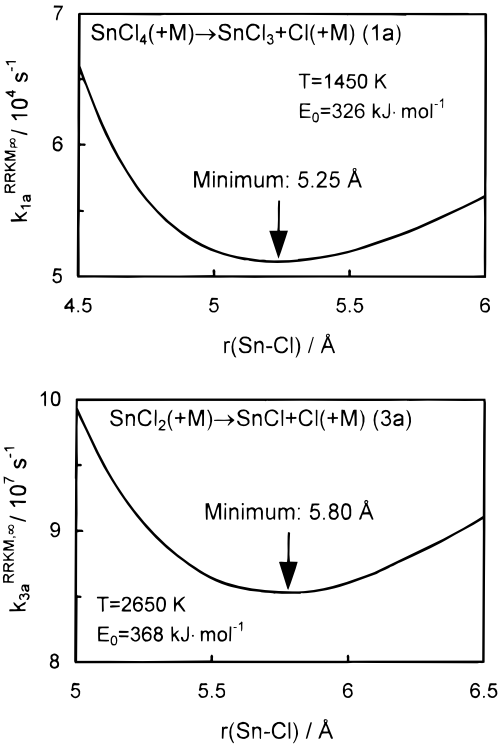

Figure 11. Variations of the RRKM high-pressure limit rate coefficients for reaction 1a (upper part) and reaction 3a (lower part) as a function of distance of the Sn−Cl bond being broken.

TABLE 3: Geometries of the Reactants and Transition States for the Reactions $SnCl_4(+Ar) \rightarrow SnCl_3 + Cl(+Ar)$ and $SnCl_2(+Ar) \rightarrow SnCl + Cl(+Ar)$

	$SnCl_4$ decomposition		$SnCl_2$ decomposition	
parameter	reactant	transition state	reactant	transition state
symmetry	T_d	C_{3v}	C_{2v}	C_s
r(Sn−Cl*)[a]/Å	2.324	5.25	2.396	5.80
r(Sn−Cl)/Å	2.324	2.357	2.396	2.410
∠(Cl*−Sn−Cl)/deg	109.5	111.5	98.4	98.4
∠(Cl−Sn−Cl)/deg	109.5	107.4		

[a] Cl* means the chlorine atom being removed through the dissociation reactions.

2250−2950 K:

$$k_{3a}^{2nd} = 10^{-8.36\pm0.86} \times \exp[-(310 \pm 42)\ \text{kJ mol}^{-1}/RT]\ \text{cm}^3\ \text{molecule}^{-1}\ \text{s}^{-1}$$

$$k_{4a}^{2nd} = 10^{-9.50\pm0.78} \times \exp[-(265 \pm 40)\ \text{kJ mol}^{-1}/RT]\ \text{cm}^3\ \text{molecule}^{-1}\ \text{s}^{-1}$$

where the error limits are at the two standard deviation level.

Obviously, both rate coefficients are smaller than k_1^{2nd}. Numerical calculations based on the kinetic data determined in the present work can reproduce not only measured Sn atom concentration, but also Cl atom concentration; see white lines in Figure 2. This confirms that the $SnCl_4$ thermal decomposition in the present study can be explained by the simplified reaction scheme consisting of reactions 1a, 2a, 3a, and 4a.

RRKM Calculations. In order to evaluate the validity of the experimental results, RRKM calculations including variational transition state theory were done for reactions 1a and 3a. The RRKM unimolecular rate coefficient $k^{RRKM,uni}$ can be expressed as follows:

TABLE 4: RRKM Parameters for the Reactions $SnCl_4(+Ar) \rightarrow SnCl_3 + Cl(+Ar)$ and $SnCl_2(+Ar) \rightarrow SnCl + Cl(+Ar)$

	$SnCl_4$ decomposition		$SnCl_2$ decomposition	
parameter	reactant	transition state	reactant	transition state
energy barrier of reaction, E_0/kJ mol^{-1}	adjusted		adjusted	
reaction path degeneracy, $l^{\ddagger}$	4		2	
Lennard-Jones parameters for the reactants σ/Å and ϵ/k_B/K	4.923, 755		4.804, 512	
Lennard-Jones parameters for Ar, σ(Ar)/Å and ϵ(Ar)/k_B/K	3.542, 93.3		3.542, 93.3	
average downward energy transferred per collision, $\langle\Delta E\rangle_{down}$/cm^{-1}	600		600	
moments of inertia for inactive external rotors/amu Å^2	510.7 (2)	1178.2 (2)	342.1	1164.1
			233.3	1016.0
moments of inertia for active external and internal rotors/amu Å^2	510.4	511.5	108.8	148.1
		335.3 (2)		205.9
vibrational frequencies/cm^{-1}	394 (3)	369 (2)	346	336
	351	345	338	
	119 (3)	121	118	
	92 (2)	99 (2)		

$$k^{\mathrm{RRKM,uni}} = l^{\ddagger}\frac{k_B T}{h}\frac{Q_R^{\ddagger}}{Q_R Q_a} \times \exp\left(-\frac{E_0}{RT}\right)\int_0^{\infty}\frac{\sum P(E^{\ddagger})\exp(-E^{\ddagger}/RT)}{1 + k_r/\beta_c k_d[\mathrm{M}]}\mathrm{d}\left(\frac{E^{\ddagger}}{RT}\right)$$

$$k_r = l^{\ddagger}\frac{Q_R^{\ddagger}}{Q_R}\frac{\sum P(E^{\ddagger})}{hN(E^{\ddagger} + E_0)}$$

where $l^{\ddagger}$ is the reaction path degeneracy; k_B and h are the Boltzmann and Planck constants; Q_R, $Q_R^{\ddagger}$ are partition functions of the adiabatic rotations for the reactant and the transition state, respectively; Q_a is the partition function of all active modes of the reactant; E_0 is the energy barrier of the reaction at 0 K; β_c, k_d are collision efficiency and rate coefficient for collisional deactivation; $\Sigma P(E^{\ddagger})$ is the total number of energy states of the transition state having energy $E^{\ddagger}$; and $N(E^{\ddagger}+E_0)$ is the density of energy states for the reactant having energy $E = E^{\ddagger} + E_0$.

In this model, the bond-dissociation transition state is treated as a loosely bound product-like moiety with four characteristics. First, the vibrational frequencies of $SnCl_3$ (product in reaction 1a) or SnCl (product in reaction 3a) do not change in the transition state. Second, the two external rotations with the largest moments are treated as adiabatic. Third, the residual external rotation and the two degrees of freedom representing the bending vibrations of the Cl fragment in $SnCl_3$ or SnCl are treated as completely free active internal rotors with moments of inertia fixed at that for an isolated $SnCl_3$ or SnCl product. Fourth, in order to search the structure of the transition state, the potential energy along the reaction coordinate is modeled with a Morse potential determined from the frequency representing the Sn−Cl stretching vibration and the energy barrier of the reaction, E_0. These treatments are widely accepted as a standard model for simple bond-fission reactions.[35−37] The geometries of $SnCl_4$ and $SnCl_3$ for reaction 1a or $SnCl_2$ and SnCl for reaction 3a were determined by the MP2/3-21G(d) ab initio MO calculations. The vibrational frequencies were also computed at the MP2/3-21G(d) level and scaled by a factor of 0.94 to compensate for known systematic errors.[38]

The high-pressure limit rate coefficients, $k_{1a}^{\mathrm{RRKM},\infty}$ and $k_{3a}^{\mathrm{RRKM},\infty}$, were calculated as a function of the separation distance of the Sn−Cl bond, r(Sn−Cl), to determine the structures of the transition states. A typical example is shown in Figure 11. The geometries at r_{1a}(Sn−Cl) = 5.25 Å and r_{3a}(Sn−Cl) = 5.80 Å, where the $k_{1a}^{\mathrm{RRKM},\infty}$ and $k_{3a}^{\mathrm{RRKM},\infty}$ have minimum values, respectively, were treated as the structures of the transition states for reactions 1a and 3a. Geometries of the reactants and transition states are listed in Table 3. All parameters required for the RRKM calculations are summarized in Table 4. For each reaction, the energy barrier of the reaction, E_0, which is the most sensitive parameter in the calculations, was adjusted until the RRKM rate coefficient matched our experimental data. The average downward energy transferred per collision, $\langle\Delta E\rangle_{down}$, is also unknown. This value ranges from 400 to 800 cm^{-1} for usual thermal decompositions.[39] In this calculation, the average value (600 cm^{-1}) was used. The value of $\langle\Delta E\rangle_{down}$ does not need to be estimated more precisely, because E_0 is much more sensitive for the rate coefficient than $\langle\Delta E\rangle_{down}$ and an error due to $\langle\Delta E\rangle_{down}$ is canceled. The solid lines in Figures 4 and 9 show the RRKM results calculated with $E_{0,1a} = 326$ kJ mol^{-1} and $E_{0,3a} = 368$ kJ mol^{-1} for reactions 1a and 3a, respectively. The fittings to our experimental data are good for both reactions. Arrhenius expressions of the high-pressure limit and the weak collision low-pressure limit rate coefficients obtained from the RRKM calculations are summarized in Table 5.

TABLE 5: Arrhenius Expressions of High-Pressure Limit and Weak Collision Low-Pressure Limit Rate Coefficients Obtained from RRKM Calculations[a]

	high-pressure limit		low-pressure limit (WC)		
reaction	A/s^{-1}	E_a/kJ mol^{-1}	A/cm^3 molecules^{-1} s^{-1}	E_a/kJ mol^{-1}	temp/K
(1a)	$10^{16.11}$	316	$10^{-7.13}$	213	1250−1700
(3a)	$10^{14.93}$	355	$10^{-8.76}$	285	2250−2950

[a] Rate coefficients in the form $k = A\exp(-E_a/RT)$.

The values of the energy barriers $E_{0,1a} = 326$ kJ mol^{-1} and $E_{0,3a} = 368$ kJ mol^{-1} obtained from the fittings are in excellent agreement with the bond dissociation energies of $SnCl_4$ and $SnCl_2$, D(Cl−$SnCl_3$) = 314 kJ mol^{-1} [22] and D(Cl−SnCl) = 370 kJ mol^{-1}.[23] These agreements lead to the conclusion that the experimental results for k_{1a} and k_{3a} are also supported by the RRKM calculations.

The experimental results for k_{4a} cannot be checked with the RRKM theory, because the theory does not support the thermal decomposition reactions of diatomic molecules. The relation of the experimental determined activation energies between reactions 3a and 4a is $E_{3a} < E_{4a}$. This tendency looks reasonable,

because the calculated reaction enthalpies have the same relation, as shown in Table 2. However, the reason the preexponential factor of k_{4a} is a power of 10 smaller than that of k_{3a} is still unknown and should be resolved in future work.

Conclusions

The present study on kinetics of the thermal decomposition of $SnCl_4$ can be summarized as follows:

(a) $SnCl_4$ finally decomposes into $Sn(^3P)$ and four chlorine atoms through the four subsequent elementary steps: $SnCl_4(+M) \rightarrow SnCl_3(^2A_1) + Cl(+M)$ (1a), $SnCl_3(^2A_1)(+M) \rightarrow SnCl_2(^1A_1) + Cl(+M)$ (2a), $SnCl_2(^1A_1)(+M) \rightarrow SnCl(^2\Pi) + Cl(+M)$ (3a), and $SnCl(^2\Pi)(+M) \rightarrow Sn(^3P) + Cl(+M)$ (4a).

(b) The rate coefficient for reaction 1a was found to be in the falloff region fairly close to the low-pressure limit. The second-order rate coefficient was experimentally determined to be $k_{1a}^{2nd} = 10^{-5.37\pm0.62} \exp[-(285 \pm 18)\ \text{kJ mol}^{-1}/RT]\ \text{cm}^3\ \text{molecule}^{-1}\ \text{s}^{-1}$ from the initial formation of Cl atoms over the temperature range of 1250−1700 K.

(c) The second-order rate coefficients for the subsequent reactions 3a and 4a were given to be $k_{3a}^{2nd} = 10^{-8.36\pm0.86} \exp[-(310 \pm 42)\ \text{kJ mol}^{-1}/RT]\ \text{cm}^3\ \text{molecule}^{-1}\ \text{s}^{-1}$ and $k_{4a}^{2nd} = 10^{-9.50\pm0.78} \exp[-(265 \pm 40)\ \text{kJ mol}^{-1}/RT]\ \text{cm}^3\ \text{molecule}^{-1}\ \text{s}^{-1}$ by detecting Sn atoms over the temperature range of 2250−2950 K.

(d) The experimental results for k_{1a} and k_{3a} were also supported by the RRKM calculations.

Acknowledgment. The authors thank Ms. N. Schlösser and Mr. L. Jerig for their help in conducting the experiments. One of the authors (Dr. K. Takahashi) expresses his gratitude to the Alexander von Humboldt Stiftung for the financial support during his stay in Germany.

References and Notes

(1) Jarzebski, Z. M.; Marton, J. P. *J. Electrochem. Soc.* **1976**, 199C.
(2) Jarzebski, Z. M.; Marton, J. P. *J. Electrochem. Soc.* **1976**, 299C.
(3) Jarzebski, Z. M.; Marton, J. P. *J. Electrochem. Soc.* **1976**, 333C.
(4) Chowdhury, M. A.; Husain, D. *J. Chem. Soc., Faraday Trans. 2* **1978**, *74*, 1065.
(5) Wiesenfeld, J. R.; Yuen, M. J. *J. Phys. Chem.*, **1978** *82*, 1225.
(6) Zaslonko, I. S.; Smirnov, V. N. *Kinet. Catal.* **1980** *21*, 602.
(7) Fontijn, A.; Bajaj, P. N. *J. Phys. Chem.* **1996** *100*, 7085.
(8) Felder, W.; Fontijn, A. *J. Chem. Phys.* **1978** *69*, 1112.
(9) Price, S. J. W.; Trotman-Dickenson, A. F. *Trans. Faraday Soc.* **1958**, *54*, 1630.
(10) Johnson, R. P.; Price, S. J. W. *Can. J. Chem.* **1972**, *50*, 50.
(11) Taylor, J. E.; Milazzo, T. S. *J. Phys. Chem.* **1978**, *82*, 847.
(12) Moller, W.; Mozzhukhin, E.; Wagner, H. Gg. *Ber. Bunsen-Ges. Phys. Chem.* **1986**, *90*, 854.
(13) Aleksandrov, Yu. A.; Baryshnikov, Yu. Yu.; Zakharov, I. L.; Lazareva, T. I. *Kinet. Catal.* **1990**, *31*, 637.
(14) Catoire, L.; Woiki, D.; Roth, P. *Int. J. Chem. Kinet.* **1997**, *29*, 415.
(15) Herzler, J.; Roth, P. *J. Chem. Phys. A* **1997**, *101*, 9341.
(16) Kunz, A.; Roth, P. *Twenty-seventh Symposium (International) on Combustion*; The Combustion Institute: Pittsburgh, PA, 1998; p 261.
(17) Woiki, D.; Roth, P. *Shock Waves.* **1994**, *4*, 95.
(18) Thielen, K.; Roth, P. *Twentieth Symposium (International) on Combustion*; The Combustion Institute: Pittsburgh, PA, 1984; p 685.
(19) Lim, K. P.; Michael, J. V. *J. Chem. Phys.* **1993** *98*, 3919.
(20) Davidson, D. F.; Chang, A. Y.; Di Rosa, M. D.; Hanson, R. K. *J. Quant. Spectrosc. Radiat. Transfer* **1993** *49*, 559.
(21) *Gaussian 94W*, Revision D.3; Frisch, M. J.; Trucks, G. W.; Schlegel, H. B.; Gill, P. M. W.; Johnson, B. G.; Robb, M. A.; Cheeseman, J. R.; Keith, T.; Petersson, G. A.; Montgomery, J. A.; Raghavachari, K.; Al-Laham, M. A.; Zakrzewski, V. G.; Ortiz, J. V.; Foresman, J. B.; Cioslowski, J.; Stefanov, B. B.; Nanayakkara, A.; Challacombe, M.; Peng, C. Y.; Ayala, P. Y.; Chen, W.; Wong, M. W.; Andres, J. L.; Replogle, E. S.; Gomperts, R.; Martin, R. L.; Fox, D. J.; Binkley, J. S.; Defrees, D. J.; Baker, J.; Stewart, J. P.; Head-Gordon, M.; Gonzalez, C.; Pople, J. A. Gaussian, Inc.: Pittsburgh, PA, 1995.
(22) Purcell, K. F.; Kotz, J. C. In *Inorganic Chemistry*; W. B. Saunders: Philadelphia, PA, 1977; p 270.
(23) Oldershaw, G. A.; Robinson, K. *J. Chem. Soc., Sect. A* **1971**, 2963.
(24) Francisco, J. S.; Li, Z. *J. Phys. Chem.* **1989**, *93*, 8118.
(25) Hiraoka, H.; Hardwick, R. *J. Chem. Phys.* **1962**, *36*, 1715.
(26) Jacobs, T. A.; Giedt, R. R. *J. Chem. Phys.* **1963**, *39*, 749.
(27) Diesen, R. W.; Felmlee, W. J. *J. Chem. Phys.* **1963**, *39*, 2115.
(28) Schfield, D.; Tsang, W.; Bauer, S. H. *J. Chem. Phys.* **1965**, *42*, 2132.
(29) von Thiel, M.; Seery, D. J.; Bitton, D. *J. Phys. Chem.* **1965**, *69*, 834.
(30) Carabetta, R. A.; Palmer, H. B. *J. Chem. Phys.* **1967**, *46*, 1333.
(31) Huybrechts, G.; Narmon, M.; van Mele, B. *Int. J. Chem. Kinet.* **1996**, *28*, 27.
(32) Baulch, D. L.; Duxbury, J.; Grant, S. J.; Montague, D. C. *J. Phys. Chem. Ref. Data* **1981**, *10*, Suppl.
(33) Kee, R. J.; Rupley, F. M.; Miller, J. A. *Chemkin-II: A Fortran Chemical Kinetics Package for the Analysis of Gas-Phase Chemical Kinetics*; Sandia National Laboratories Report SAND89-8009; Sandia Laboratories: Albuquerque, NM, 1993.
(34) Lutz, A. E.; Kee, R. J.; Miller, J. A. *SENKIN: A Fortran Program for Predicting Homogeneous Gas-Phase Chemical Kinetics with Sensitivity Analysis*; Sandia National Laboratories Report SAND87-8248; Sandia Laboratories: Albuquerque, NM, 1991.
(35) Benson, S. W.; Golden, D. M. In *Physical Chemistry, An Advanced Treatise*; Eyring, H., Henderson, D., Jost, W., Eds.; Academic Press: New York, 1975; Vol. VII.
(36) Smith, G. P.; Manion, J. A.; Rossi, M. J.; Rodgers, A. S.; Golden, D. M. *Int. J. Chem. Kinet.* **1994**, *26*, 211.
(37) Kumaran, S. S.; Lim, K. P.; Michael, J. V.; Wagner, F. A. *J. Chem. Phys.*, **1995** *99*, 8673.
(38) Foresman, J. B.; Frisch, M. J. *Exploring Chemistry with Electronic Structure Methods*, 2nd ed.; Gaussian, Inc.: Pittsburgh, PA, 1996; p 64.
(39) Tsang, W. *Combust. Flame* **1989**, *78*, 71.